Carbohydrate Polymers 157 (2017) 344–352

Contents lists available at ScienceDirect

Carbohydrate Polymers

journal homepage: www.elsevier.com/locate/carbpol

Flexible polypyrrole/copper sulfide/bacterial cellulose nanofibrous composite membranes as supercapacitor electrodes

Shuo Peng [a], Lingling Fan [b,*], Chengzhuo Wei [a], Xiaohong Liu [a], Hongwei Zhang [a], Weilin Xu [a,b], Jie Xu [a,*]

[a] College of Materials Science & Engineering, State Key Lab for New Textile Materials & Advanced Processing Technology, Wuhan Textile University, 430200, Wuhan, China
[b] College of Textile Science & Engineering, Wuhan Textile University, 430200, Wuhan, China

ARTICLE INFO

Article history:
Received 15 September 2016
Received in revised form 2 October 2016
Accepted 3 October 2016
Available online 4 October 2016

Keywords:
Polypyrrole
Copper sulfide
Bacterial cellulose
Nanofibrous composite membranes
Flexible supercapacitor

ABSTRACT

Polypyrrole (PPy) and copper sulfide (CuS) have been successfully deposited on bacterial cellulose (BC) membranes to prepare nanofibrous composite electrodes of PPy/CuS/BC for flexible supercapacitor applications. The introduction of CuS remarkably improves the specific capacitance and cycling stability of BC-based electrodes. The specific capacitance of the supercapacitors based on the PPy/CuS/BC electrodes can reach to about 580 F g^{-1} at a current density of 0.8 mA cm^{-2} and can retain about 73% of their initial value after 300 cycles, while the PPy/BC-based device could retain only 21.7% after 300 cycles. This work provides a promising approach to fabricate cost-effective and flexible nanofibrous composite membranes for high-performance supercapacitor electrodes.

1. Introduction

Recently, wearable electronics and their associated technologies have been envisioned in an array of applications, thus greatly boosting the developments of flexible and wearable energy storage systems (Jost, Dion, & Gogotsi, 2014). Flexible supercapacitors have received considerable attention due to their desirable advantages, such as high energy density, good cycling stability, fast charge/discharge rate, and environmental safety (Firoz Babu, Siva Subramanian, & Anbu Kulandainathan, 2013; Liang et al., 2013; Xu et al., 2013; Li, Huang, Yang et al., 2014; Li, Huang, Zhang et al., 2014; Liu, Yu, Yan, Li, & Zheng, 2015; Qin et al., 2015; Xu, Wang, & Fan, 2015; Xu, Wang, Yuan, Wei, & Duan, 2015; Xu, Wang, Yuan, Wei, & Gu, 2015; Zhu et al., 2014). On the basis of the energy-storage mechanisms and the used electrode materials, supercapacitors can be divided into electrical double layer capacitors (EDLCs) and pseudocapacitors. The energy stored in EDLCs mainly results from the charge separation at the electrode/electrolyte interface, and the electrode materials used in EDLCs are carbon materials. Usually, carbon materials have good rate capability but exhibit a relatively small specific capacitance. The main electrode materials used for pseudocapacitors are transition metal oxides/sulfides and conducting polymers (CPs, e.g. polypyrrole (PPy), polyaniline, polythiophene and their derivatives). Pseudocapacitor materials have relatively large capacitance values because the energy is stored through a reversible redox reaction.

Among the abovementioned electrode materials, CPs have promised the most for high-performance flexible supercapacitor applications due to their high conductivity, high intrinsic flexibility, various preparation methods and nontoxicity (Gholami, Nia, & Alias, 2015; Liu, He, Fan, Miao, & Liu, 2014; Lü, Chen, Lin, & Yu, 2015; Mensing, Wisitsoraat, Phokharatkul, Lomas, & Tuantranont, 2015; Ramya, Sivasubramanian, & Sangaranarayanan, 2013; Snook, Kao, & Best, 2011; Wang, Li, Ni, Dai, & Lu, 2015). On the basis of low cost and environmental stability, PPy and PPy-based composites used for flexible supercapacitors have been intensively studied. For example, Firoz Babu et al. (2013) investigated the influence of the fabric substrates on electrochemical performance and reported a specific capacitance of 235 F g^{-1} for their viscose-based PPy electrode. Zhao and coworkers (Zhao, Shu, Wang, Gambhir, & Wallace, 2015) demonstrated the performance of PPy-graphene-coated nylon lycra textile electrode in supercapacitor application, showing a specific capacitance of 114 F g^{-1} at a scan rate of 5 mV s^{-1}. Liu, Cai, Zhao, Zhao, & Ge, 2016 fabricated a

* Corresponding authors.
E-mail addresses: hglingling@126.com (L. Fan), xujie0@ustc.edu (J. Xu).

http://dx.doi.org/10.1016/j.carbpol.2016.10.004
0144-8617/

PPy/multi-walled carbon nanotube (MWCNT)/cotton flexible electrode, which exhibited a specific capacitance of 535 F g^{-1} at a very low scan rate of 1 mV s^{-1}. Despite the attractive electrochemical performance and potential of CNTs and graphene, the relatively high price of CNTs and elaborate procedures to obtain graphene would impede their further development in large-scale fabrication.

Transition metal sulfides (e.g., CuS, NiS, CoS, and VS) have been considered as one of the most promising pseudocapacitor materials with respect to their specific capacitance and cost effectiveness (Feng et al., 2011; Hsu, Chen, & Lin, 2014; Peng et al., 2015; Raj et al., 2014; S. Liu et al., 2015; Zhu, Xia, Zhou, & Lou, 2012;). In the recent past, CuS have been extensively investigated due to their good electronic conductivity and high energy capacitance. For example, Zhu et al. (2012) utilized the template-engaged chemical conversion route to prepare CuS nanoneedles on carbon nanotube as electrode, which exhibited a specific capacitance of 122 F g^{-1} in KOH electrolyte. More recently, Hsu et al. (2014) have fabricated a CuS nanowire (NW) array with a hierarchical nanoarchitecture on copper foil using a simple liquid-solid reaction, achieving a specific capacitance of 305 F g^{-1} at a current density of 0.6 mA cm^{-2}. Combining PPy with CuS to form composite electrode materials for flexible supercapacitors is an effective route to further improve the electrochemical properties of supercapacitors. However, to the best of our knowledge, composite materials of PPy and CuS for flexible supercapacitors have rarely been reported.

Bacterial cellulose (BC) is a fascinating natural nanofibrous material with a three-dimensional and interconnected network structure, which can be produced on industrial scales through microbial fermentation process. The average diameter of its ribbon-like fibrils is lower than 100 nm, while the length can be larger than 100 μm. The specific structure and numerous hydrogen bonds endow BC with sufficient porosity and high specific surface area, which can serve as a matrix to support other functionalized materials and a template to form different nanostructures (Hu, Chen, Yang, Zhe, & Wang, 2014; Tang, Han, Jiang, Chen, & Wang, 2015). For example, CdS and CdSe nanoparticles have been prepared on the BC nanofibers using in situ precipitation method (Li et al., 2009; Yang et al., 2012). PPy (Müller, Rambo, Recouvreux, Porto, & Barra, 2011; Müller, Rambo, Porto, Schreiner, & Barra, 2013; Wang, Bian, Zhou, Tang, & Tang, 2013) and PANI (Lee, Chung, Kwon, Kim, & Tze, 2012; Marins et al., 2011; Müller et al., 2012) nanoparticles have been synthesized on the BC nanofibers via in-situ polymerization. Recently, Tang et al. prepared the polysiloxane-coated PPy/BC nanocomposite membranes with amphiphobicity by in situ oxidative polymerization of PPy and then infiltrated with polysiloxane solution (Tang et al., 2015). In our previous work (Xu et al., 2013), we have successfully fabricated the PPy/BC nanofibrous membranes with core-sheath structure for the application of flexible supercapacitor electrodes, which exhibited an initial capacitance of 459.5 F g^{-1} at 0.16 A g^{-1} current density. More recently, the PPy/NiS/BC membranes were prepared in our group (Peng et al., 2016), which had a relatively high initial capacitance of 713 F g^{-1} at 0.8 mA cm^{-2} current density. However, the capacitance was decreased dramatically during the charge/discharge cycles, with the remaining capacitance of 258 F g^{-1} (only 36.2% of the initial value) and 172 F g^{-1} (24.2%) after 100 and 300 cycles, respectively. CuS could provide good cycling durability due to the crystallinity of CuS (Raj et al., 2014). To improve the cycling performance of the BC-based electrodes, herein, we report the fabrication of flexible PPy/CuS/BC nanofibrous composite membranes, which exhibited a high specific capacitance as high as 580 F g^{-1} and good cycling performance (the retention 73% of initial specific capacitance after 300 cycles) at a current density of 0.8 mA cm^{-2}.

2. Experimental

2.1. Materials

BC membranes (food-grade, degree of polymerization $\approx 5.18 \times 10^3$) were purchased from Hainan Yide Foods Co. Ltd. (China) and treated as the previous report (Xu et al., 2013). Other chemicals were supplied by Sinopharm Chemical Reagent Co. Ltd. (China) and used as received. Ultrapure water used in the experiments with resistivity of 18 MΩ cm was produced a Milli-Q Advantage system.

2.2. In situ synthesis of CuS on BC nanofibers

In a typical procedure, the purified BC membrane (4 × 4 cm) were immersed into a beaker with a magnetic stirring bar containing 50 mL aqueous solution of copper sulfate pentahydrate ($CuSO_4 \cdot 5H_2O$) for 8 h. Then it was taken out and soaked into a 50 mL aqueous solution of sodium sulfide (Na_2S) with the same concentration as $CuSO_4$ solution for 1 min. It was observed that the BC membrane changed to a dark green color. Finally, the membrane was washed with pure water for several times and dried in a vacuum oven at 60 °C for 12 h. The BC membranes treated by the solutions of $CuSO_4 \cdot 5H_2O$ with different concentrations of 10, 50, 100 mM were named as CuS/BC-10, CuS/BC-50 and CuS/BC-100, respectively.

2.3. Fabrication of PPy/CuS/BC composite membranes

PPy was deposited on the CuS/BC membranes through in-situ oxidative polymerization as previously reported (Xu et al., 2013). The CuS/BC membranes were soaked in a pyrrole aqueous solution (1.0 M) and stirred for 1 h. An aqueous solution of iron (III) chloride hexahydrate ($FeCl_3 \cdot 6H_2O$, 0.5 M) was added to initiate the polymerization. After 2 h at 5 °C, the obtained samples were cleaned thoroughly with alcohol and pure water and dried in a vacuum oven at 40 °C for 12 h. The composites prepared on different CuS/BC membranes were coded as PPy/CuS/BC-10, PPy/CuS/BC-50 and PPy/CuS/BC-100, respectively. The control sample obtained by using purified BC membrane without CuS was named as PPy/BC.

2.4. Characterization

The mass of active materials was determined by the weight difference before and after the deposition of CuS and PPy. The microscopic features of the samples were characterized on a JSM-6510LV scanning electron microscopy (SEM) microscope (JEOL, Japan). Energy dispersive X-ray spectroscopy (EDS) was examined on a HORIBA X-ACT spectrometer. Fourier transform infrared (FTIR) spectra were recorded by a TGA-FTIR spectrometer (Tensor 27, Bruker, Germany) equipped with attenuated total reflectance (ATR) cell. Thermal gravimetric analysis (TGA) was carried out under nitrogen atmosphere with a TG209F1 thermogravimetric analyzer (NETZSCH, Germany) at a heating rate of 10 °C min^{-1}. The surface conductivity was measured by a digital four-point probe resistivity measurement system (RTS-9, 4Probes Tech. Co., China) with copper electrodes under a pressure of 5 N.

The electrochemical properties of the membrane electrodes were measured based on a symmetric two-electrode system with 2.0 M sodium chloride (NaCl) aqueous solution as electrolyte and a filter paper as separator. Cyclic voltammetry (CV) and electrochemical impedance spectroscopy (EIS) were recorded with an Autolab PGSTAT302N electrochemical workstation (Metrohm AG, Switzerland). The CV measurements were carried out from −0.9 V

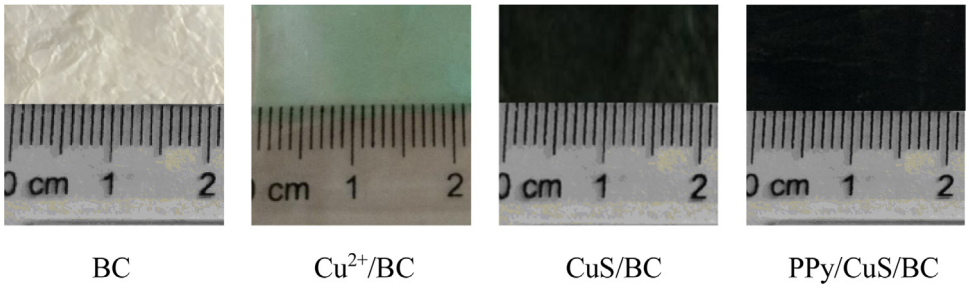

Fig. 1. Optical images of BC, Cu2+/BC, CuS/BC and PPy/CuS/BC membranes.

to +0.9 V at various scan rates. The EIS tests were carried out in the frequency range from 0.01 Hz to 100 kHz using a sine wave with alternate signal amplitude of 5 mV. Galvanostatic charge-discharge (GCD) cycling measurements were conducted over the potential range from 0 to 0.8 V on a multichannel LAND CT2001A battery testing device (Wuhan Land Electronics, China).

3. Results and discussion

The images of BC and BC composites are shown in Fig. 1. Firstly, when the BC membrane was soaked in $CuSO_4$ solution, the guest Cu^{2+} ions could infuse into the three-dimensional network structure through the nanopores of BC to reach adsorption equilibrium. The Cu^{2+} ions were anchored on the surface of the BC membrane by the electrostatic interactions between Cu^{2+} and cellulose, since the oxygen atoms can bind Cu^{2+} by sharing a lone pair of electrons (Hu, Chen, Zhou, Wang, 2010). The free Cu^{2+} can be eliminated by washing in water. The BC membrane turned from white to light green, suggesting the steady adsorption of Cu^{2+} on the membrane. As being dipped into the Na_2S solution, CuS was produced quickly owing to the strong interaction between Cu^{2+} and S^{2-}, and the color of the samples changed to dark green quickly.

The microscopic features of the BC and CuS/BC membranes were investigated by SEM and the images are provided in Fig. 2. The BC nanofibers have an average diameter less than 100 nm and are cross-linked and overlapped, forming a porous three-dimensional network (Fig. 2a). The characteristic structure provides a valuable feature for the adsorption and distribution of Cu^{2+} on the BC nanofibers. For the CuS/BC-10 membrane obtained with dilute $CuSO_4$ solution, the appearance of frequent grooves, wrinkles and roughness on the surface and interspaces of the BC nanofibers indicated the successful deposition of CuS onto the BC membrane (Fig. 2b). When the $CuSO_4$ concentration increased, the aggregated CuS particles were observed on the BC membranes (Fig. 2c and 2d). The EDS patterns of the CuS/BC-50 membrane (Fig. 2e) further confirm the presence of CuS on the BC membrane.

The FTIR spectra of the BC, Cu^{2+}/BC-50 and CuS/BC-50 composites are plotted in Fig. 3a. For BC (Müller et al., 2013), the bands at 3340 and 2895 cm^{-1} were attributed to the stretching vibration of hydroxyl groups and the asymmetrically stretching vibration of C—H and CH_2, respectively. The in-plane OH deformation and bending vibrations were observed at 1647 and 1315 cm^{-1}, respectively. The peak of the C—O asymmetric bridge stretching situated at 1159 cm^{-1}. The intensive bands at 1107 and 1055 cm^{-1} corresponded to the skeletal vibration of the C—O and C—O—C functional groups of the pyranose ring. After the adsorption of Cu^{2+}, the bands corresponding to the in-plane OH deformation and bending vibrations became relatively strong in the spectrum of the Cu^{2+}/BC membrane. This observation pointed out that there was a stable interaction between the OH groups and the Cu^{2+} ions and these groups were the reactive position during in situ synthesis (Li et al., 2009). Since the ATR infrared light can penetrate only a filmy layer, it could be inferred that the CuS coatings on the BC was quite thin from the appearance of the typical peaks of cellulose in the spectrum of the CuS/BC membrane.

As shown in Fig. 3b, TGA had been performed for BC, CuS/BC-10, and CuS/BC-100 membranes. The weight loss had been monitored as a function of temperature. For BC, the first period from 25 °C to 250 °C with about 13% weight loss was attributed to the dehydration of cellulose. The drastic weight loss in the second period (250–380 °C) was ascribed to the destruction of cellulose into d-glucopyranose and free radical. The weight loss during the third stage from 380 – 600 °C was caused by the decarboxylation and decarbonylation reactions. The CuS/BC composites underwent a similar weight loss manner. However, the water loss in the composite membranes was decreased with the introduction of CuS. In addition, the onset temperature of the second stage for the CuS/BC membranes was lower than that for pure BC, indicating that the composite membranes are less thermally stable than pure BC. These results can be ascribed to that the hydrogen bonds in BC were probably broken by the interaction between BC and CuS. The lower weight loss of the composites than BC was due to the CuS residue.

The FTIR spectrum of PPy/CuS/BC-50 shown in Fig. 3a primarily presented the typical peaks of PPy, revealing that the BC nanofibers were entirely overlapped by PPy due to its high thickness (Peng et al., 2016). The peaks at 1524 cm^{-1} and 1435 cm^{-1} were attributed to the C—C and C—N stretching vibrations in the pyrrole ring, respectively. The peak at 1283 cm^{-1} corresponded to the C—H and N—H in-plane deformation modes. The breathing vibration of the PPy ring appeared at 1130 cm^{-1}. The mode of in-plane deformation vibration of NH_2^+ groups derived from the protonated PPy chains was observed at 1084 cm^{-1} (Omastová, Trchová, Kovářová, & Stejskal, 2003). The peak at 1007 cm^{-1} was assigned to the C—H and N—H in-plane deformation vibrations. The C—C and C—H out-of-plane ring deformation modes were located at 959 and 764 cm^{-1}, respectively. Comparing to the FTIR spectrum of the PPy/BC membrane reported previously (Xu et al., 2013), the characteristic peaks of PPy shifted obviously to lower wavenumbers in the PPy/CuS/BC-50 composite possibly owing to the interaction between the PPy chain and the CuS layer.

The BC membrane is not conductive with a sheet resistance more than 10^{15} Ω sq^{-1}; however, the membrane could become conductive after the introduction of CuS, with the conductivity of about 0.5 S cm^{-1}. With the PPy coatings, the conductivity of the composite membranes further increased to 8.2, 6.9, and 5.1 S cm^{-1} for PPy/CuS/BC-10, PPy/CuS/BC-50 and PPy/CuS/BC-100, respectively, which is even higher than those of PPy/BC membrane (3.9 S cm^{-1}) (Xu et al., 2013), pure PPy film (1.14 S cm^{-1}) (Wang et al., 2010), PPy-Cladophora cellulose composite paper (slightly above 1 S cm^{-1}) (Nyström, Razaq, Strømme, Nyholm, & Mihranyan, 2009), and PPy/graphene-coated cotton fabric (1.2 S cm^{-1}) (Xu, Wang, Yuan, Wei, & Duan, 2015). The conductivity of the composite membranes decreased with the increasing CuS concentration, perhaps due to the relatively low conductivity of CuS as compared

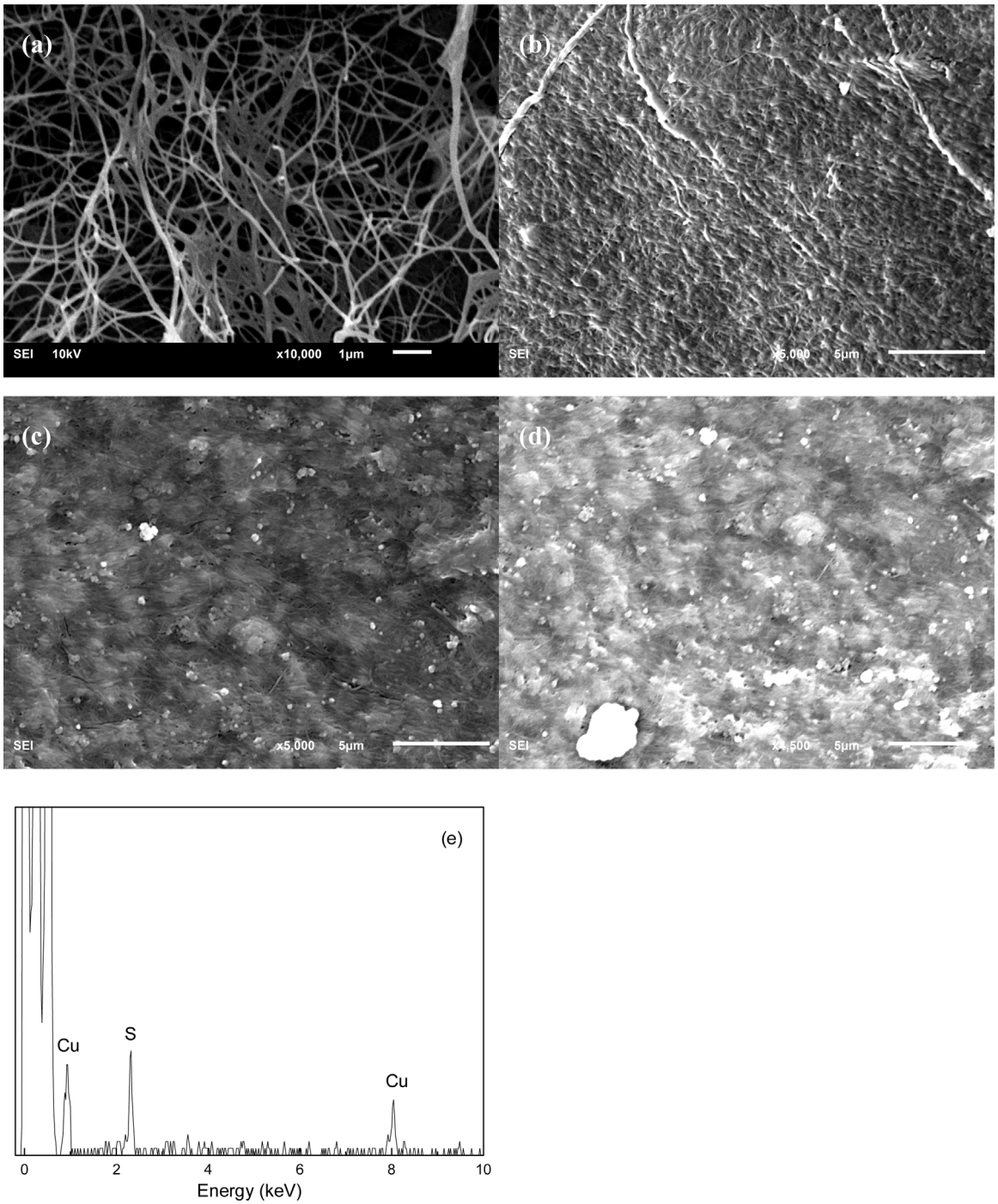

Fig. 2. SEM images of (a) BC and CuS/BC membranes: (b) CuS/BC-10, (c) CuS/BC-50 and (d) CuS/BC-100; (e) EDS pattern of the CuS/BC-50 membrane.

with PPy. The high conductivity confirmed the possible application of the composite membranes in flexible electronics. In addition, the color of BC membranes changed from dark green to black after the polymerization (Fig. 1).

The SEM images of the PPy/BC and PPy/CuS/BC samples are given in Fig. 4. For all the samples, the PPy nanoparticles were mostly formed along the BC nanofibers to construct a continuous nanosheath structure as well as some aggregations. As the CuS layer on the nanofibers was rather flimsy and the nanofibers were not entirely overlapped, it can be inferred that pyrrole could permeate through the CuS layer and contact the nanofibers. The hydrogen bonds could act as a traction force to support the growing of the PPy nanosheath on the BC nanofibers and prevent the formation of aggregates (Xu et al., 2013). Meanwhile, the CuS layer between the nanofibers was destroyed significantly by the growing of PPy. The composite membranes were flexible enough to be bent by 180° without breaking (shown in the inset of Fig. 4d), and be folded and released for many times. The excellent flexibility of the resultant membranes and excellent adhesion of PPy is attributable to the formation of hydrogen bonding because of the effective interactions between the imine groups of PPy and the hydroxyl groups of cellulose. The nanosheath structure, high conductivity and excellent flexibility make the PPy/CuS/BC composite membranes promising flexible electrode materials for supercapacitors.

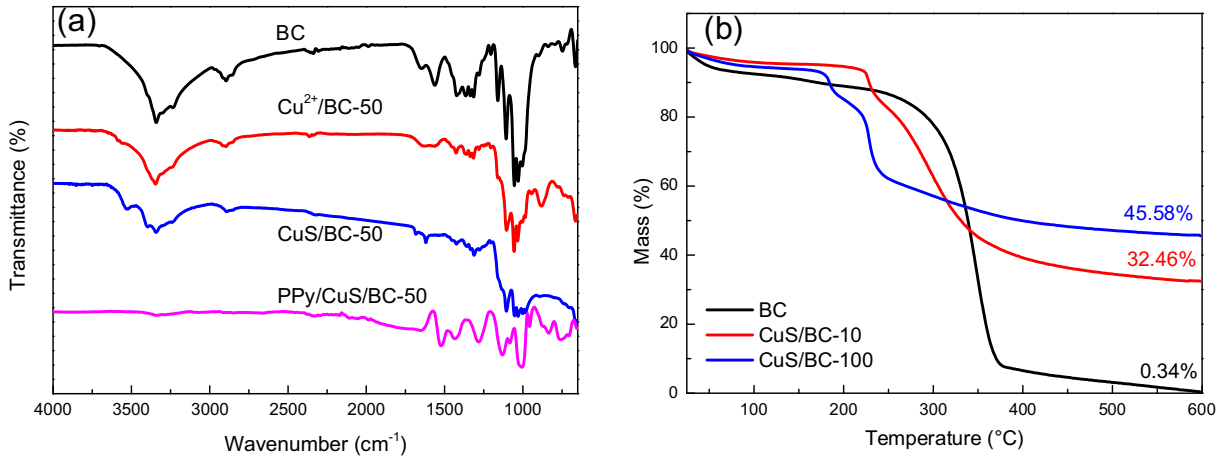

Fig. 3. (a) FTIR spectra of BC, Cu^{2+}/BC-50, CuS/BC-50 and PPy/CuS/BC-50 membranes; (b) TG curves of pure BC, CuS/BC-10, and CuS/BC-100 membranes.

As a useful experimental tool with small potential variation, EIS is more reliable for characterizing the frequency response of the supercapacitor and it can provide the electronic/ionic conductivity of the electrode materials during the charge-discharge progress. Fig. 5a presents the Nyquist plots for the PPy/BC and PPy/CuS/BC electrodes. All the impedance plots were featured by a semicircle in the high frequency region and a linear portion in the low frequency region. The interception of the semicircle at the real axis in the high frequency region represents the internal resistance related to the intrinsic resistance of the active materials and the electrolytic resistance. The linear portion corresponds to the diffusion-limited process, suggesting an ideal capacitive behavior. The equivalent series resistance (R_s) values for PPy/CuS/BC-10 (9.5 Ω) and PPy/CuS/BC-50 (10.1 Ω) were slightly lower than that for PPy/BC (11.2 Ω) and PPy/CuS/BC-100 (12.1 Ω), revealing that the electrical conductivity of overall electrode was reduced by the deposition of less CuS. Such an increase in the electrical conductivity of the BC-based supercapacitor can improve electrochemical performance, which can play a key role in enhancing the power density. In the low frequency region, the impedance curves of the PPy/CuS/BC-50 electrodes were less parallel to the imaginary axis as compared with the other electrodes, indicating the proper addition of CuS in the PPy/CuS/BC-50 electrodes was favorable for the infiltration of electrolyte ion to some extent (Yang et al., 2016). Fig. 5b shows the cyclic voltammetry (CV) curves for the PPy/BC and PPy/CuS/BC-50 membranes at a scan rate of 5 mV s^{-1} with the potential window ranging from −0.9 V to 0.9 V. Nearly rectangular shapes with large enclosed area were observed and there were no obvious redox peaks for the PPy/BC and PPy/CuS/BC-50 membranes, indicating that the electrodes were charged and discharged at a pseudo-constant rate over the whole CV process. The devices based on the PPy/CuS/BC-50 membranes had a higher area than

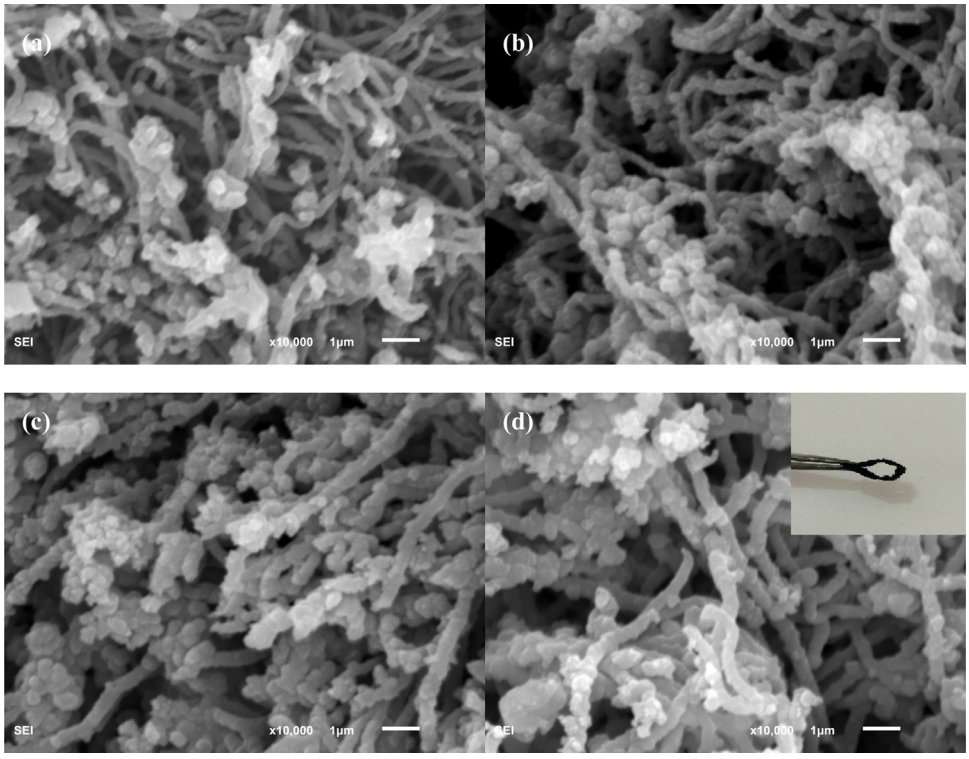

Fig. 4. SEM images of (a) PPy/BC and PPy/CuS/BC membranes: (b) PPy/CuS/BC-10, (c) PPy/CuS/BC-50 and (d) PPy/CuS/BC-100.

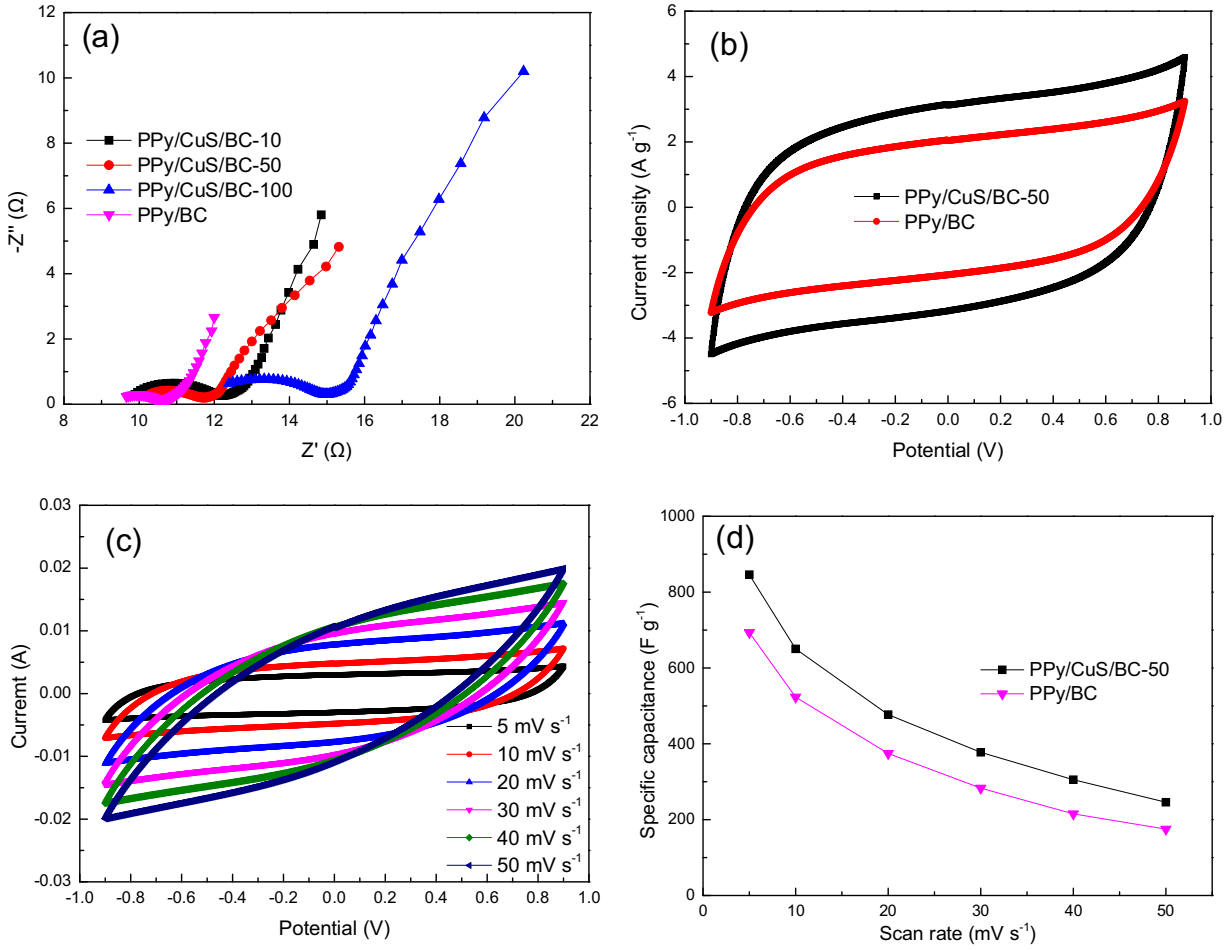

Fig. 5. (a) Nyquist plots of the supercapacitors based on PPy/BC and PPy/CuS/BC electrodes; (b) CV curves of the supercapacitors based on PPy/CuS/BC-50 and PPy-BC electrodes at a scan rate of 5 mV s^{-1}; (c) CV curves of the supercapacitors based on PPy/CuS/BC-50 electrode at different scan rates; (d) Specific capacitance calculated from CV curves for the supercapacitors based on PPy/CuS/BC-50 and PPy-BC electrodes at different scan rates.

the PPy/BC-based sample in the CV curves. In general, the enclosed area of the CV curve is proportional to the specific capacitance of the electrode material. The CV curves for the PPy/CuS/BC-50 sample at different scan rates are presented in Fig. 5(c). With the increased scan rates, the CV profiles for the samples deviated from rectangle-like shape. Based on the CV curves, the specific capacitance (C_{sp}) can be calculated by the following equation:

$$C_{sp} = \frac{\int IdV}{v \times \Delta V \times m}$$

where I is the response current, v is the scan rate, ΔV is the voltage window, and m is the mass of the active materials. The calculated C_{sp} values for PPy/BC and PPy/CuS/BC-50 at different scan rates are shown in Fig. 5(d). The C_{sp} for the PPy/CuS/BC-50 and PPy/BC samples at the scan rate of 5 mV s^{-1} was 846 and 693 F g^{-1}, respectively. The capacitance of PPy/CuS/BC-50 was higher than that of PPy/BC due to the synergetic contributions from the pseudocapacitance of PPy and CuS. The C_{sp} values decreased gradually with the increase of scan rates because of the ion diffusion effect within the active materials and at the electrode/electrolyte interface (Wang et al., 2012).

The GCD curves of the supercapacitors based on the PPy/CuS/BC and PPy-BC electrodes were tested at different current densities. An ideal supercapacitor will exhibit the symmetrical triangle shapes of the GCD curves with small *IR* drops, revealing that the redox reaction is reversible. The *IR* drop is usually caused by the overall internal resistance of the devices. Low internal resistance is of great importance in energy-storage devices as less energy will be wasted to produce unwanted heat during GCD processes (Zhong et al., 2015). It can be found from Fig. 6a that the GCD curves were almost symmetrical at a current density of 0.8 mA cm^{-2}. The supercapacitors based on the PPy/CuS/BC electrodes had relatively smaller *IR* drops than that based on the PPy/BC electrodes at the same current density, indicating that the supercapacitors based on the PPy/CuS/BC electrodes have better capacitive property. The gram-specific capacitance (C_m) can be calculated from the GCD curves with the following equation:

$$C_m = \frac{I \times t}{(\Delta V - IR_{drop}) \times m}$$

where I is the constant charge/discharge current, t is the discharge time, ΔV is the potential window, IR_{drop} is the IR voltage drop, and m is the mass of electroactive material in the working electrode. The C_m values for PPy/CuS/BC-10, PPy/CuS/BC-50 and PPy/CuS/BC-100 at a current density of 0.8 mA cm^{-2} were calculated to be about 530, 580 and 575 F g^{-1}, respectively, exceeding the value for PPy/BC (502 F g^{-1}). The maximum value for PPy/CuS/BC-50 is even larger than the reported values of BC-based electrodes, such as PPy/BC/MWCNT (216.4 F g^{-1}) (Li, Huang, Yang et al., 2014) and chemically bonded PPy/BC/graphene composites (556 F g^{-1}) (Liu, Zhou, Tang, & Tang, 2015). The mass loading of active materials for the PPy/BC membranes were significantly larger than that for the composite membranes, leading to larger total capacitance and consequently longer discharge time. However, the higher thick-

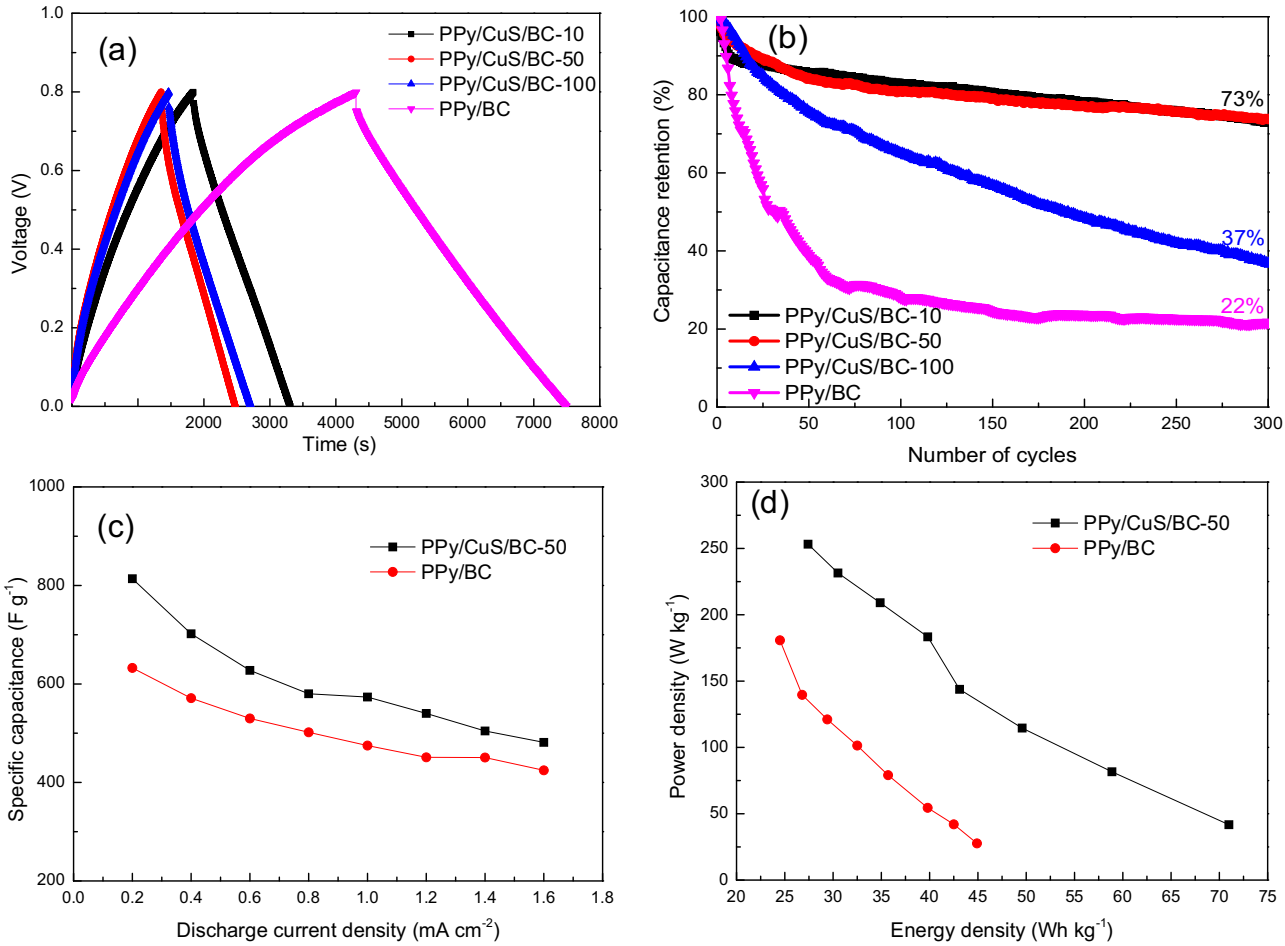

Fig. 6. (a) Galvanostatic charge-discharge profiles of the supercapacitors based on PPy/CuS/BC and PPy-BC electrodes at a current density of 0.8 mA cm^{-2}; (b) Cycling stability at a current density of 0.8 mA cm^{-2}; (c) Specific capacitance of the supercapacitors based on PPy/CuS/BC-50 and PPy-BC electrodes at different current densities; (d) Ragone plots of the supercapacitors based on PPy/CuS/BC-50 and PPy-BC electrodes.

ness of the PPy/BC membranes caused a decrease in flexibility as compared with the composite membranes. Cycling performance of the electrodes was evaluated by long-term GCD, as shown in Fig. 6b. The devices based on the PPy/CuS/BC-10, PPy/CuS/BC-50 and PPy/CuS/BC-100 electrodes could retain 73%, 73% and 37% of their initial C_m after 300 cycles, respectively, while the PPy/BC-based device could retain only 22% of its initial C_m after 300 cycles. The remaining specific capacitance of 423 F g^{-1} for PPy/CuS/BC-50 is about 2.5 times of that for the recently proposed PPy/NiS/BC (172 F g^{-1}) after 300 cycles (Peng et al., 2016). The capacitance loss of the PPy materials has been demonstrated to arise from the volume swelling and the structure relaxation of the materials caused by the intercalation and dissociation of dopant anions during the long-time charge and discharge processes. The CuS layer served as frameworks to stabilize the PPy layer and to limit the swelling and shrinking of the PPy coating during the charge/discharge runs, thus leading to an improved cycling stability. It is noteworthy that the device based on PPy/CuS/BC-100 had relatively poorer stability than those based on PPy/CuS/BC-10 and PPy/CuS/BC-50 perhaps due to the degradation of CuS layer in PPy/CuS/BC-100. Further improvement on the cycling stability is needed for potential applications. Nevertheless, due to their low cost and facile fabrication, the PPy/CuS/BC composites show promising applications in wearable electronics when apparel is changed frequently. The C_m values for the devices based on PPy/CuS/BC-50 and PPy/BC at different current densities are shown in Fig. 6c. It can be found that the C_m values decreased with the increase of the current densities. The capacitance of the device based on PPy/CuS/BC-50 was retained 59.2% when the current density increases from 0.2 A cm^{-2} to 1.6 A cm^{-2}. The specific capacitance of the device based on PPy/CuS/BC-50 at the current density of 1.6 A cm^{-2} was still quite large, being about 481 F g^{-1}. The specific energy density (E) and power density (P) can be calculated by the following formulas (Xing et al., 2006):

$$E = (1/2)CV^2$$

$$P = E/t$$

where C corresponds to the capacitance of the two-electrode capacitor, V is the potential window (excluding IR drop at the beginning of the discharge), and t is the discharge time. The Ragone plots for the devices based on PPy/CuS/BC-50 and PPy-BC are shown in Fig. 6d. It is obvious that the supercapacitor based on PPy/CuS/BC-50 exhibited better performances. The power density can reach to about 253 W kg^{-1}, and the energy density can reach to about 71.0 Wh kg^{-1} for the supercapacitor based on PPy/CuS/BC-50. However, the device based on PPy/BC had obviously small energy densities and power densities due to the low C_m values and larger IR drops during the GCD process. The energy density in the present work is significantly larger than the reported values for the devices using the PPy-coated fabrics (Liang et al., 2013; Xu, Wang, & Fan, 2015; Xu, Wang, Yuan, Wei, & Gu, 2015; Zhu et al., 2014) and the PPy/RGO-coated fabrics (Xu, Wang, Yuan, Wei, & Duan, 2015) due to the synergetic contributions from the pseudocapacitance of PPy and

CuS. The data suggest that the PPy/CuS/BC membranes are expected to be used for high-performance supercapacitors.

4. Conclusions

PPy/CuS/BC nanofibrous composite membranes have been successfully prepared in this work. The obtained PPy/CuS/BC membranes are highly conductive to be directly used as flexible supercapacitor electrodes. Electrochemical tests demonstrate that the introduction of CuS could improve the capacitive performances. The supercapacitors based on the PPy/CuS/BC electrodes can achieve a relatively high specific capacitance of about 580 F g^{-1} at a current density of 0.8 mA cm^{-2} and can retain 73% of their initial capacitance after 300 cycles. This study shows a promising potential to fabricate flexible, cost-effective and high-performance nanofibrous composite membranes for supercapacitor applications.

Acknowledgements

The authors thank the financial support from Scientific Innovation Team Project of the Education Department of Hubei Province (No. T201507), Natural Science Foundation of China (No. 51325306) and Hubei Province (No. 2012FFA098), Application and Foundation Research Project of Wuhan Science and Technology Bureau of China (No. 2016010101010016), and Hubei Key Laboratory of Low Dimensional Optoelectronic Material and Devices (No. HLOM142005).

References

Feng, J., Sun, X., Wu, C., Peng, L., Lin, C., Hu, S., et al. (2011). Metallic few-layered VS_2 ultrathin nanosheets: High two-dimensional conductivity for in-plane supercapacitors. *Journal of the American Chemical Society*, *133*, 17832–17838.

Firoz Babu, K., Siva Subramanian, S. P., & Anbu Kulandainathan, M. (2013). Functionalisation of fabrics with conducting polymer for tuning capacitance and fabrication of supercapacitor. *Carbohydrate Polymers*, *94*, 487–495.

Gholami, M., Nia, P. M., & Alias, Y. (2015). Morphology and electrical properties of electrochemically synthesized pyrrole- formyl pyrrole copolymer. *Applied Surface Science*, *357*, 806–813.

Hsu, Y. K., Chen, Y. C., & Lin, Y. G. (2014). Synthesis of copper sulfide nanowire arrays for high-performance supercapacitors. *Electrochimica Acta*, *139*, 401–407.

Hu, W., Chen, S., Zhou, B., & Wang, H. (2010). Facile synthesis of ZnO nanoparticles based on bacterial cellulose. *Materials Science and Engineering B*, *170*, 88–92.

Hu, W., Chen, S., Yang, J., Zhe, L., & Wang, H. (2014). Functionalized bacterial cellulose derivatives and nanocomposites. *Carbohydrate Polymers*, *101*, 1043–1060.

Jost, K., Dion, G., & Gogotsi, Y. (2014). Textile energy storage in perspective. *Journal of Materials Chemistry A*, *2*, 10776–10787.

Lü, Q.-F., Chen, G., Lin, T.-T., & Yu, Y. (2015). Dye-functionalized graphene/polyaniline nanocomposite as an electrode for efficient electrochemical supercapacitor. *Composites Science and Technology*, *115*, 80–86.

Liu, L., Yu, Y., Yan, C., Li, K., & Zheng, Z. (2015). Wearable energy-dense and power-dense supercapacitor yarns enabled by scalable graphene–metallic textile composite electrodes. *Nature Communications*, *6*, 7620.

Lee, H.-J., Chung, T.-J., Kwon, H.-J., Kim, H.-J., & Tze, W. T. Y. (2012). Fabrication and evaluation of bacterial cellulose-polyaniline composites by interfacial polymerization. *Cellulose*, *19*, 1251–1258.

Li, X., Chen, S., Hu, W., Shi, S., Shen, W., Zhang, X., et al. (2009). In situ synthesis of CdS nanoparticles on bacterial cellulose nanofibers. *Carbohydrate Polymers*, *76*, 509–512.

Li, S., Huang, D., Yang, J., Zhang, B., Zhang, X., Yang, G., et al. (2014). Freestanding bacterial cellulose-polypyrrole nanofibres paper electrodes for advanced energy storage devices. *Nano Energy*, *9*, 309–317.

Li, S., Huang, D., Zhang, B., Xu, X., Wang, M., Yang, G., et al. (2014). Flexible supercapacitors based on bacterial cellulose paper electrodes. *Advanced Energy Materials*, *4*, 1301655.

Liang, G., Zhu, L., Xu, J., Fang, D., Bai, Z., & Xu, W. (2013). Investigations of poly(pyrrole)-coated cotton fabrics prepared in blends of anionic and cationic surfactants as flexible electrode. *Electrochimica Acta*, *103*, 9–14.

Liu, M., He, S., Fan, W., Miao, Y. E., & Liu, T. (2014). Filter paper-derived carbon fiber/polyaniline composite paper for high energy storage applications. *Composites Science and Technology*, *101*, 152–158.

Liu, C., Cai, Z., Zhao, Y., Zhao, H., & Ge, F. (2016). Potentiostatically synthesized flexible polypyrrole/multi-wall carbon nanotube/cotton fabric electrodes for supercapacitors. *Cellulose*, *23*, 637–648.

Müller, D., Rambo, C. R., Recouvreux, D. O. S., Porto, L. M., & Barra, G. M. O. (2011). Chemical in situ polymerization of polypyrrole on bacterial cellulose nanofibers. *Synthetic Metals*, *161*, 106–111.

Müller, D., Mandelli, J. S., Marins, J. A., Soares, B. G., Porto, L. M., Rambo, C. R., et al. (2012). Electrically conducting nanocomposites: Preparation and properties of polyaniline (PAni)-coated bacterial cellulose nanofibers (BC). *Cellulose*, *19*, 1645–1654.

Müller, D., Rambo, C. R., Porto, L. M., Schreiner, W. H., & Barra, G. M. O. (2013). Structure and properties of Polypyrrole/Bacterial cellulose nanocomposites. *Carbohydrate Polymers*, *94*, 655–662.

Marins, J. A., Soares, B. G., Dahmouche, K., Ribeiro, S. J. L., Barud, H., & Bonemer, D. (2011). Structure and properties of conducting bacterial cellulose-polyaniline nanocomposites. *Cellulose*, *18*, 1285–1294.

Mensing, J. P., Wisitsoraat, A., Phokharatkul, D., Lomas, T., & Tuantranont, A. (2015). Novel surfactant-stabilized graphene-polyaniline composite nanofiber for supercapacitor applications. *Composites Part B: Engineering*, *77*, 93–99.

Nyström, G., Razaq, A., Strømme, M., Nyholm, L., & Mihranyan, A. (2009). Ultrafast all-polymer paper-based batteries. *Nano Letters*, *9*, 3635–3639.

Omastová, M., Trchová, M., Kovářová, J., & Stejskal, J. (2003). Synthesis and structural study of polypyrroles prepared in the presence of surfactants. *Synthetic Metals*, *138*, 447–455.

Peng, L., Ji, X., Wan, H., Ruan, Y., Xu, K., Chen, C., et al. (2015). Nickel sulfide nanoparticles synthesized by microwave-assisted method as promising supercapacitor electrodes: An experimental and computational study. *Electrochimica Acta*, *182*, 361–367.

Peng, S., Fan, L., Wei, C., Bao, H., Zhang, H., Xu, W., et al. (2016). Polypyrrole/nickel sulfide/bacterial cellulose nanofibrous composite membranes for flexible supercapacitor electrodes. *Cellulose*, *23*, 2639–2651.

Qin, K., Kang, J., Li, J., Shi, C., Li, Y., Qiao, Z., et al. (2015). Free-standing porous carbon nanofiber/ultrathin graphite hybrid for flexible solid-state supercapacitors. *ACS Nano*, *9*, 481–487.

Raj, C. J., Kim, B. C., Cho, W. J., Lee, W. G., Seo, Y., & Yu, K. H. (2014). Electrochemical capacitor behavior of copper sulfide (CuS) nanoplatelets. *Journal of Alloys and Compounds*, *586*, 191–196.

Ramya, R., Sivasubramanian, R., & Sangaranarayanan, M. V. (2013). Conducting polymers-based electrochemical supercapacitors-progress and prospects. *Electrochimica Acta*, *101*, 109–129.

Liu, S., Mao, C., Niu, Y., Yi, F., Hou, J., Lu, S., et al. (2015). Facile synthesis of novel networked ultralong cobalt sulfide nanotubes and its application in supercapacitors. *ACS Applied Materials & Interfaces*, *7*, 25568–25573.

Snook, G. A., Kao, P., & Best, A. S. (2011). Conducting-polymer-based supercapacitor devices and electrodes. *Journal of Power Sources*, *196*, 1–12.

Tang, L., Han, J., Jiang, Z., Chen, S., & Wang, H. (2015). Flexible conductive polypyrrole nanocomposite membranes based onbacterial cellulose with amphiphobicity. *Carbohydrate Polymers*, *117*, 230–235.

Wang, D., Li, Y.-X., Shi, Z., Qin, H.-L., Wang, L., Pei, X.-F., et al. (2010). Spontaneous growth of free-standing polypyrrole films at an air/ionic liquid interface. *Langmuir*, *26*, 14405–14408.

Wang, Z.-L., Guo, R., Li, G.-R., Lu, H.-L., Liu, Z.-Q., Xiao, F.-M., et al. (2012). Polyaniline nanotube arrays as high-performance flexible electrodes for electrochemical energy storage devices. *Journal of Materials Chemistry*, *22*, 2401–2404.

Wang, H., Bian, L., Zhou, P., Tang, J., & Tang, W. (2013). Core–sheath structured bacterial cellulose/polypyrrole nanocomposites with excellent conductivity as supercapacitors. *Journal of Materials Chemistry A*, *1*, 578–584.

Wang, J., Li, B., Ni, T., Dai, T., & Lu, Y. (2015). One-step synthesis of iodine doped polyaniline-reduced graphene oxide composite hydrogel with high capacitive properties. *Composites Science and Technology*, *109*, 12–17.

Xing, W., Qiao, S. Z., Ding, R. G., Li, F., Lu, G. Q., Yan, Z. F., et al. (2006). Superior electric double layer capacitors using ordered mesoporous carbons. *Carbon*, *44*, 216–224.

Xu, J., Zhu, L., Bai, Z., Liang, G., Liu, L., Fang, D., et al. (2013). Conductive polypyrrole–bacterial cellulose nanocomposite membranes as flexible supercapacitor electrode. *Organic Electronics*, *14*, 3331–3338.

Xu, J., Wang, D., Fan, L., Yuan, Y., Wei, W., Liu, R., et al. (2015). Fabric electrodes coated with polypyrrole nanorods for flexible supercapacitor application prepared via a reactive self-degraded template. *Organic Electronics*, *26*, 292–299.

Xu, J., Wang, D., Yuan, Y., Wei, W., Duan, L., Wang, L., et al. (2015). Polypyrrole/reduced graphene oxide coated fabric electrodes for supercapacitor application. *Organic Electronics*, *24*, 153–159.

Xu, J., Wang, D., Yuan, Y., Wei, W., Gu, S., Liu, R., et al. (2015). Polypyrrole-coated cotton fabrics for flexible supercapacitor electrodes prepared using CuO nanoparticles as template. *Cellulose*, *22*, 1355–1363.

Liu, Y., Zhou, J., Tang, J., & Tang, W. (2015). Three-dimensional chemically bonded polypyrrole/bacterial cellulose/graphene composites for high-performance supercapacitors. *Chemistry of Materials*, *27*, 7034–7041.

Yang, Z., Chen, S., Hu, W., Yin, N., Zhang, W., Xiang, C., et al. (2012). Flexible luminescent CdSe/bacterial cellulose nanocomoposite membranes. *Carbohydrate Polymers*, *88*, 173–178.

Yang, C., Zhang, L., Hu, N., Yang, Z., Wei, H., & Zhang, Y. (2016). Reduced graphene oxide/polypyrrole nanotube papers for flexible all-solid-state supercapacitors with excellent rate capability and high energy density. *Journal of Power Sources*, *302*, 39–45.

Zhao, C., Shu, K., Wang, C., Gambhir, S., & Wallace, G. G. (2015). Reduced graphene oxide and polypyrrole/reduced graphene oxide composite coated stretchable fabric electrodes for supercapacitor application. *Electrochimica Acta*, *172*, 12–19.

Zhong, J., Fan, L. Q., Wu, X., Wu, J. H., Liu, G. J., Lin, J. M., et al. (2015). Improved energy density of quasi-solid-state supercapacitors using sandwich-type redox-active gel polymer electrolytes. *Electrochimica Acta*, *166*, 150–156.

Zhu, T., Xia, B., Zhou, L., & Lou, X. W. D. (2012). Arrays of ultrafine CuS nanoneedles supported on a CNT backbone for application in supercapacitors. *Journal of Materials Chemistry*, *22*, 7851–7855.

Zhu, L., Wu, L., Sun, Y., Li, M., Xu, J., Bai, Z., et al. (2014). Cotton fabrics coated with lignosulfonate-doped polypyrrole for flexible supercapacitor electrodes. *RSC Advances*, *4*, 6261–6266.